Ultramicroscopy 50 (1993) 285–299
North-Holland

ultramicroscopy

# Accurate measurements of mean inner potential of crystal wedges using digital electron holograms

M. Gajdardziska-Josifovska [a,1], M.R. McCartney [a], W.J. de Ruijter [a,2], David J. Smith [a,b], J.K. Weiss [a] and J.M. Zuo [b]

[a] *Center for Solid State Science, Arizona State University, Tempe, AZ 85287, USA*
[b] *Department of Physics, Arizona State University, Tempe, AZ 85287, USA*

Received 8 February 1993; in final form 3 June 1993

The mean inner potential of a solid is a fundamental property of the material and depends on both composition and structure. By using cleaved crystal wedges of known angle, combined with digital recording of off-axis electron holograms and with theoretical calculations of dynamical effects, the mean inner potential of Si ($9.26 \pm 0.08$ V), MgO ($13.01 \pm 0.08$ V), GaAs ($14.53 \pm 0.17$ V) and PbS ($17.19 \pm 0.12$ V) is measured with high accuracy of about 1%. Dynamical contributions to the phase of the transmitted beam are found by Bloch wave calculations to be less than 5% when the crystal wedges are tilted away from zone-axis orientations and from major Kikuchi bands. The accuracy of the present method is a factor of 3 better than previously achieved by reflection high-energy electron diffraction and electron interferometry. The major causes of uncertainty were specimen imperfections and errors in phase measurement and magnification calibration.

## 1. Introduction

Electron holography is unique among transmission electron microscopy techniques in that it allows retrieval of the phase of the electron wave, information which is lost with other imaging techniques. With access to the phase, interactions of the incident electron wave with the electrostatic and magnetic potentials of the specimen can be studied directly with high spatial resolution [1]. This well established technique has been used to study magnetic field distributions [2], in addition to periodic [3] and mean [4] electrostatic potentials. The recent development of slow scan CCD cameras has enabled recording of digital holograms, resulting in improved quantification of phase measurements (see companion paper [5]).

By applying digital recording to holograms from cleaved crystal wedges, we have developed a method for accurate measurement of the mean inner potential of crystals [6]. In this paper we report on the details of our experiment and also present new results on experimental and theoretical studies of dynamical diffraction effects on mean inner potential measurements from crystal wedges.

### *1.1. Mean inner potential*

The volume average of the scalar potential of a solid is known as its mean inner potential. This potential is negative and has a value typically between $-5$ and $-30$ V, depending on the composition and structure of the solid. The mean inner potential is given by the zero-order Fourier coefficient ($V_0$) of the crystal potential (for infinitely large perfect crystals), and is usually taken as an ad-hoc zero of the potential. However, $V_0$ has several important meanings (see, e.g., recent review by Spence [7]). Miyake and Ibers have

[1] Present address: Department of Physics, University of Wisconsin – Milwaukee, 1900 E. Kenwood Boulevard, Milwaukee, WI 53211, USA.
[2] Present address: Department of Biochemistry and Biophysics, University of California at San Francisco, San Francisco, CA 94143-0448, USA.

shown that $V_0$ is proportional to the second moment of the charge density for an atom, and hence to Langevin's diamagnetic susceptibility for a gas [8]. More recently it was shown that $V_0$ for a crystal depends on sums of dipole and quadrupole moments in the unit cell, and methods were developed for the calculation of $V_0$ from mean square radii of the atoms ($\langle r^2 \rangle$), or from atomic structure factors for X-ray scattering [9]. The dependence on $\langle r^2 \rangle$ makes $V_0$ very sensitive to the redistribution of the outer valence electrons due to bonding: $V_0$ could be intuitively interpreted as a measure of the effective atomic sizes in a crystal. In practice $V_0$ is important in low-energy electron diffraction (LEED), reflection high-energy electron diffraction (RHEED), Fresnel imaging of interfaces, and in electron holography because it increases the effective energy of the electrons in the solid thereby defining the refraction of the transmitted and diffracted beams. Accurate methods for measuring $V_0$ are therefore of considerable interest.

### *1.2. Refraction effects: electron diffraction methods*

In the LEED literature the so-called inner potential is frequently confused with the constant part of the "muffin-tin" potential (see, e.g., discussion by Van Hove et al. [10]). However, the precise definition of the *inner potential* as the depth of the average potential well felt by LEED electrons in the absence of strong diffraction effects [11] is identical to the definition of the *mean inner potential* in high-energy electron diffraction or holography. The inner potential is a parameter in many LEED measurements: to measure the surface periodicities from a LEED pattern, the positions of the diffracted spots need to be corrected for substantial refraction effects which are governed by the inner potential; to measure the relaxation or contraction of the crystal planes parallel to the surface, the inner potential is a parameter in the LEED $I$–$V$ curve-fitting calculations. Although LEED experiments provide a basis for the measurement of the inner potential no tables of values have been produced. This is mainly due to three complications: (i) strong diffraction effects are impossible to avoid in LEED; (ii) there is a surface contribution to the bulk inner potential which is due to the limited penetration depth of low-energy electrons; (iii) corrections for electron exchange and correlation effects are needed at low electron energies.

In the case of high-energy electron diffraction, the refraction effects are pronounced only at small angles of incidence of the electrons with respect to the crystal surface. This situation is due to the large difference between the value of the mean inner potential $V_0$ and the kinetic energy of the incident electrons $E$ ($E \gg V_0$), which results in an index of refraction $n$ that is only slightly larger than one [12]:

$$n = \frac{K}{k} = 1 + \frac{e|V_0|}{E} \frac{E_0 + E}{2E_0 + E}, \tag{1}$$

where $K$ is the electron wavevector in the material, $k$ is the wavevector in vacuum, $E_0$ is the rest energy and $e$ is the electron charge: for example, $n = 1.000082$ for 100 keV electrons incident on a crystal with $V_0 = 15$ V. Experimental measurements of $V_0$ have been obtained from RHEED patterns from surfaces of bulk crystals [13,14] and from transmission diffraction patterns from electron-transparent polyhedral crystals with some of their faces at small angles to the incident electrons [15]. Exchange and correlation effects are negligible in RHEED but the surface and/or diffraction effects remain.

### *1.3. Phase changes: electron interferometry and holography methods*

In addition to the change in the propagation direction, the refractive index of eq. (1) also causes a phase shift of an electron wave transmitted through a material, relative to a coherent reference wave which has only traveled through vacuum. For monoenergetic incident electrons with wavelength $\lambda$, in the absence of dynamical diffraction effects, this phase change $\Delta\phi$ depends only on the thickness of the material, $t$, and its mean inner potential [12]:

$$\Delta\phi = \frac{2\pi}{\lambda}(n-1)t = \frac{2\pi e}{\lambda E} \frac{E_0 + E}{2E_0 + E} |V_0| t$$
$$= C_E |V_0| t, \tag{2}$$

where $C_E$ is an energy-dependent constant.

This phase change has been used previously to determine the mean inner potential of films with known thickness [4]. Amorphous and polycrystalline films of desired nominal thickness have been used, deposited in the shape of strips or disks on electron-transparent substrates. The phase change was measured directly from the off-axis electron hologram (interferometric measurements), by recording the shift of a holographic fringe at the edge of the film, the distance between adjacent fringes corresponding to a phase change of $2\pi$. The reported statistical accuracies in these studies have ranged from 2.5% to 9.5%, although uncertainties in specimen thickness are very likely sources of systematic errors.

Interferometric measurements of $V_0$ have also been performed for single crystals by using samples with known shape, such as chrysotile fibers [16], MgO smoke crystals [16,17] and cleaved MgO crystals [18], with relative errors between 3.5% and 8%. In this work we perform holographic measurements for several crystal wedges of known angle, and therefore thickness gradient, prepared by cleavage along well defined crystallographic planes. The accuracy of our measurements is enhanced by recording the holograms digitally, with a slow-scan CCD camera, followed by numerical reconstruction of the phase of the exit-surface wave. Dynamical diffraction contributions are an important consideration in the case of crystalline materials [16]. We evaluate the diffraction effects by comparing theoretical Bloch wave calculations with experimental measurements for several crystal orientations.

## 2. Experimental setup

A schematic diagram of the electron microscope setup for off-axis electron holography is shown in fig. 1. A thermally assisted field emission gun was used in a Philips EM400ST-FEG transmission electron microscope operated at 100 kV. Four different materials were studied: GaAs 90° wedges with cleavage along {110} crystal planes; MgO and PbS 90° wedges with cleavage along {100} crystal planes; and Si 70.5° and 109.5°

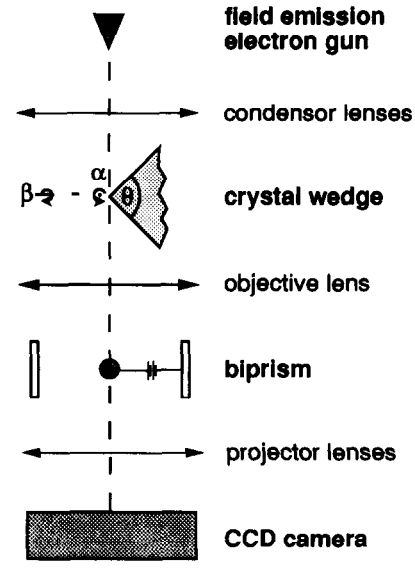


Fig. 1. Schematic drawing of setup for off-axis electron holography. Crystal wedge is tilted around two denoted axes.

wedges with cleavage along {111} crystal planes. An electron biprism was used to create the holograms which were recorded with a Gatan 679 slow-scan CCD camera equipped with a 1024 × 1024 pixel detector. Our system has been described in detail in the accompanying papers [5,19]. For the holograms presented in this paper, electron optical magnification of ~ 520k × has been used, with biprism voltages between 70 and 90 V, and CCD exposure times of 1 s. The CCD camera was also used to record CBED patterns from the crystals in order to measure their exact orientation denoted by the angles $\alpha$ and $\beta$ in fig. 1. Hologram reconstruction was performed on a VAX 3200 workstation using SEMPER.

## 3. Digital holograms and numerical reconstruction

A typical digital electron hologram from a GaAs wedge is shown in fig. 2. Holographic fringes with a periodicity of ~ 0.24 nm can be seen in the bright central band, while coarser Fresnel fringes due to the biprism wire are visible

at the edges of the hologram. Charging on the biprism can also be observed at the lower edge of the hologram, as arrowed in fig. 2. The crystal edge can be discerned in this hologram, but almost no other contrast from the crystal can be seen. The crystal was deliberately tilted away from the [100] zone axis ($\alpha = 4.15°$; $\beta = 1.95°$) in order to minimize dynamical diffraction effects, as monitored by the disappearance of extinction contours in the hologram. The tilts were further adjusted to minimize the intensity of diffraction spots in the SAD patterns and by avoiding major Kikuchi lines through the 000 disk in the CBED patterns.

The digital acquisition of the holograms enables ready use of numerical reconstruction methods. Fig. 3a shows a logarithmic display of the modulus of the Fourier transform from the hologram in fig. 2. The autocorrelation is well separated from the sidebands for tilted crystals because of the absence of high spatial frequencies in the image wave (the hexagonal spot pattern in the sideband is due to the fiber-optic array in the CCD camera). In this case, the choice of the size of the sideband is not as critical as in high-resolution holography [20], enabling use of a $256 \times 256$ pixel region centered on one of the sidebands for the subsequent reconstruction (see delineated box in fig. 3a). This region was extracted from the complex FFT and the modulus and phase of the inverse Fourier transform were calculated to obtain the images in figs. 3b and 3c, respectively. The modulus corresponds to the normal bright-field image observed in conventional electron microscopy; the phase image is used in our subsequent analysis to calculate the mean inner potential.

The main advantage of using a CCD camera in


Fig. 2. Digital electron hologram of GaAs wedge. Fine fringes in central bright region result from interference of electron wave which has passed through the crystal with coherent reference wave which has traveled through vacuum. Coarse fringes at edge of hologram are Fresnel fringes due to biprism wire. Effect of charging on wire shown arrowed.

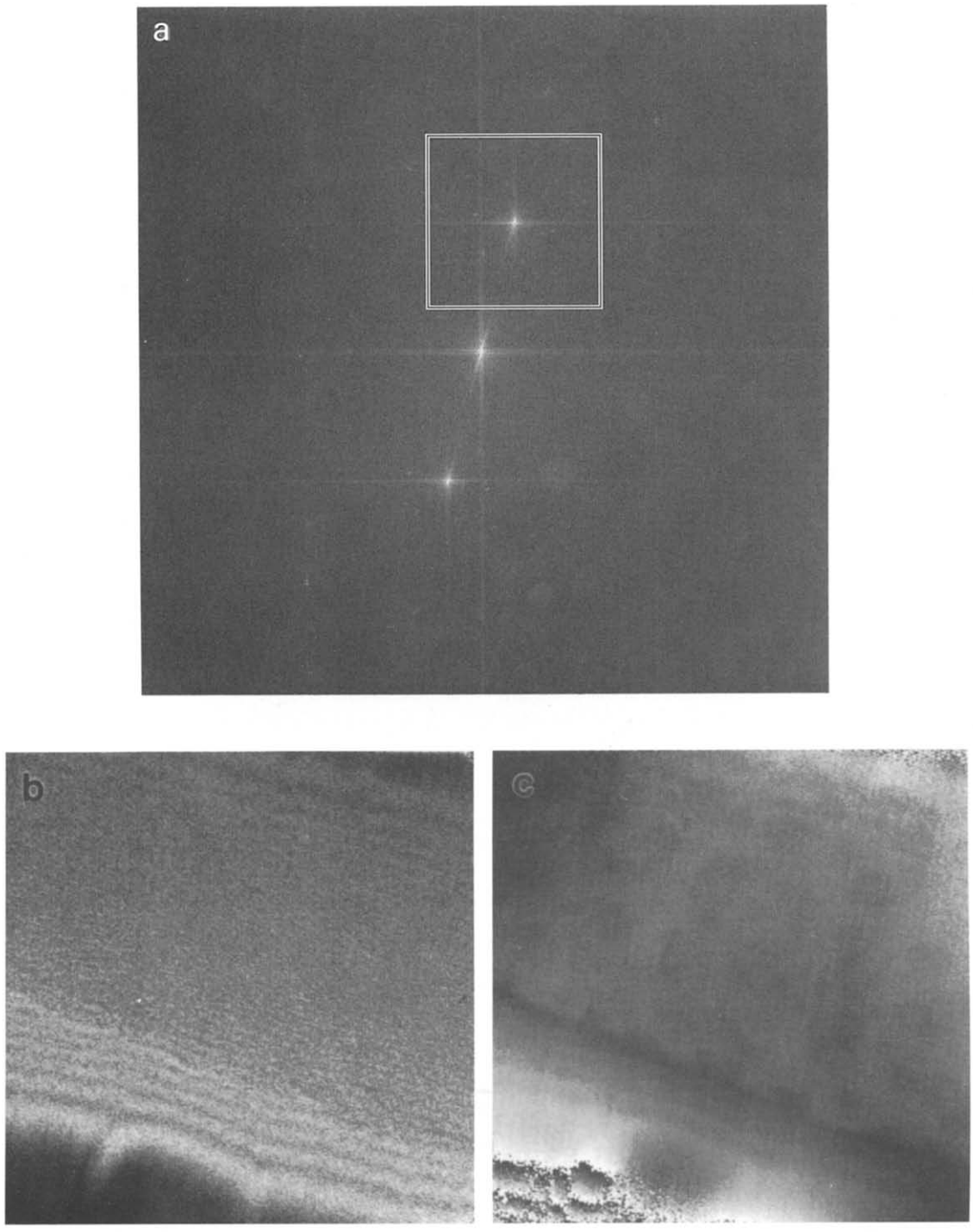


Fig. 3. (a) Fourier transform of GaAs hologram with box indicating sideband used to reconstruct modulus and phase image. (b) Modulus of GaAs image wave. (c) Phase of GaAs image wave. Note that surface pitting is more obvious in phase image.

our experiment comes from its fixed position with respect to the microscope imaging system. This allows correction of the holograms for distortions introduced by the projector lenses, to which phase images are particularly sensitive [5,21]. An example of the geometric distortion correction for the phase image of fig. 3c is shown in fig. 4. Before correction, the phase image from the GaAs wedge shows distortions in vacuum and in the crystal towards the edges of the image, which are more visible when the image is contoured with equiphase lines, as done in fig. 4a. A reference phase image, reconstructed from a hologram acquired after removal of the specimen from the beam (all the other parameters are kept unchanged), is shown in fig. 4b. The phase in this hologram of vacuum should be flat, but the contour lines at $\pi/8$ intervals delineate the distortions which are introduced by the imaging system and by charging on the biprism wire. By subtracting this phase image of vacuum from the phase image in fig. 4a we obtain the corrected image in fig. 4c. Some residual charging remains, but the flatness of the phase in vacuum is substantially improved. This is an important gain since the phase in vacuum is a reference with respect to which the phase in the specimen is measured. In the crystal, the equiphase lines (at $\pi/4$ intervals) are, on average, parallel to each other and to the edge of the sample, as one would expect from a wedge sample with linear increase in thickness. The residual waviness of the equiphase lines corresponds to the dark patches in the phase image of fig. 3b and might be attributed to surface pitting. This pitting is not visible in the reconstructed amplitude image (fig. 3b), nor was it pronounced in conventional micrographs from the same specimen.

The contributions of surface topography to measurements of the bulk mean inner potential can be minimized by phase averaging. The $200 \times 70$ pixel region shown in fig. 5a was extracted from the phase image of GaAs shown in fig. 4c. By averaging over 70 pixels along the direction parallel to the crystal edge, the phase profile given in fig. 5b was obtained. This profile shows a high level of flatness in the vacuum and a linear increase in phase in the tilted crystal wedge, except at the very edge of the wedge. This effect might be anticipated because of surface oxidation of the cleaved semiconductor and possible chipping of the crystal edge. The latter can be corrected by extrapolating the phase fit, but oxidation poses a more serious problem in determining the absolute wedge thickness which is used in eq. (2) to determine the inner potential. However,

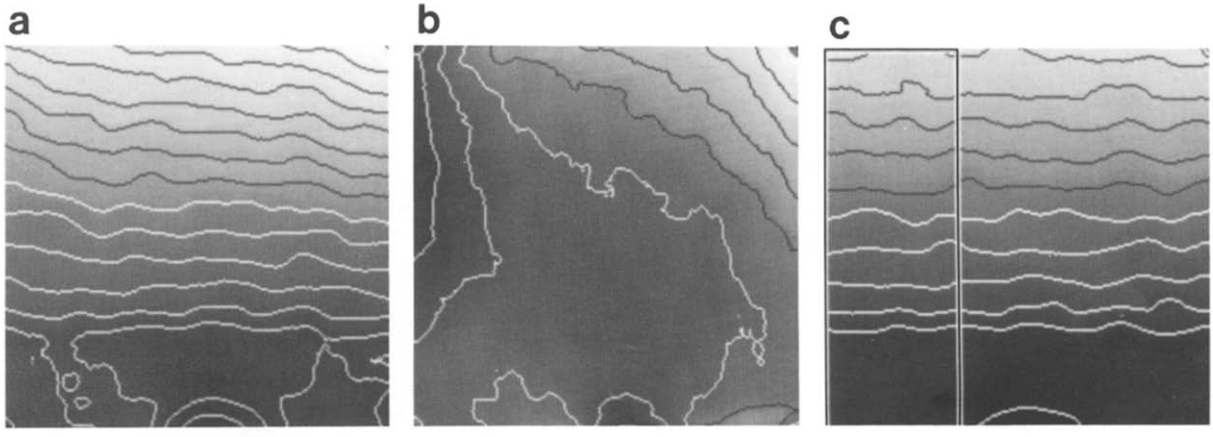


Fig. 4. (a) Phase image before geometric correction with superimposed equiphase contours at $\pi/4$ intervals (contrast of contours is inverted with respect to phase image for better visibility). Note "non-flatness" of vacuum and curvature of phase lines in crystal wedge. (b) Phase image of vacuum with equiphase contours at $\pi/8$ intervals shows distortions due to imaging system. (c) Distortion-corrected phase image with contours at $\pi/4$ intervals obtained by subtracting (b) from (a). Box marks region used for phase averaging.

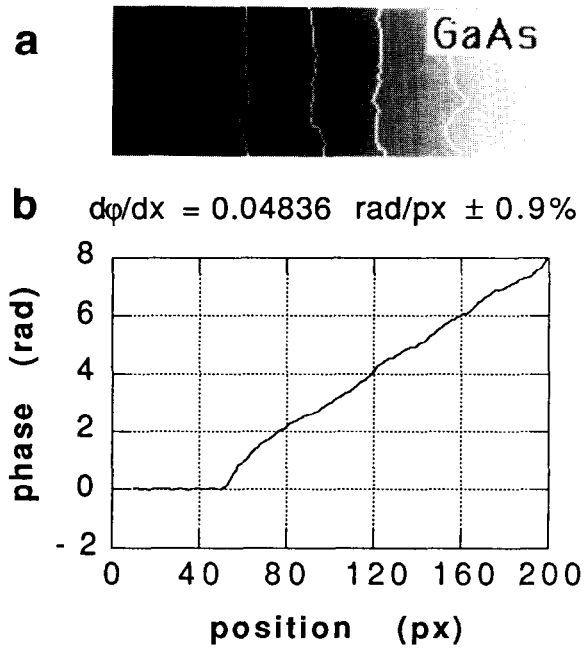


Fig. 5. (a) 70×200 pixel region extracted from phase image of GaAs wedge ($\theta = 90°$; $\alpha = 4.15°$; $\beta = 1.95°$). (b) Phase profile obtained by averaging along the direction parallel to the crystal edge. Phase averaging minimizes contribution of surface topography to measurements of bulk mean inner potential and increases signal-to-noise ratio.

overlayers of uniform thickness, such as an amorphous oxide in our case, or reconstructions on clean surfaces, introduce a constant phase change which would not contribute to the slope of the phase profile in fig. 5b.

## 4. Calculation of $V_0$ using kinematical approximation

Eq. (2) can be rearranged to express the bulk mean inner potential in terms of the change in phase and the change in thickness with position:

$$|V_0| = \frac{1}{C_E} \frac{\mathrm{d}\Delta\phi/\mathrm{d}x}{\mathrm{d}t/\mathrm{d}x}. \tag{3}$$

The change of the projected thickness of a wedge with position depends upon its orientation with respect to the incident electron beam (angles $\alpha$ and $\beta$ denoted in fig. 1), as well as the electron-optical magnification of the microscope ($M$). If the wedge angle is $\theta$, $\mathrm{d}t/\mathrm{d}x$ can be deduced from simple geometry to be:

$$\frac{\mathrm{d}t}{\mathrm{d}x} = M \frac{\tan\left(\frac{1}{2}\theta - \alpha\right) + \tan\left(\frac{1}{2}\theta + \alpha\right)}{\cos\beta}. \tag{4}$$

The parameters $C_E$, $(\mathrm{d}\Delta\phi/\mathrm{d}x)$, $M$, $\alpha$ and $\beta$ in eqs. (3) and (4) must be determined experimentally, and the errors in their measurement contribute to the final error in the calculated mean inner potential.

The magnification was calibrated using digital high-resolution images from the GaAs wedge recorded at the same objective and projector lens currents used for the electron holograms. From precise measurements of the {200} lattice fringes of GaAs, using a Hanning window in real space followed by bi-linear interpolation in reciprocal space [22], the magnification in the reconstructed phase image was determined to be $M = 0.1830 \pm 0.0004$ nm/pixel. The angles of tilt for the crystal were measured from digital convergent beam diffraction patterns to be $\alpha = 4.15°$ and $\beta = 1.95°$ with a negligible relative error of about 0.05%.

The energy-dependent constant $C_E$ in eq. (2) also contributes very little to the uncertainty of the final result. For the microscope used in this experiment, the energy of the electrons at the nominal 100 keV has been determined from detailed analysis of high-order Laue zone lines in convergent beam electron diffraction patterns to be $E = 99.96 \pm 0.02$ keV [23]. The constant calculated with this energy value was $C_E = 9.245 \times 10^6$ rad/V · m with a relative error of less than 0.01%.

For the tilted GaAs crystal (figs. 2–5) the linear fit to the phase profile in the specimen (fig. 5b) yields a slope of $\mathrm{d}\Delta\phi/\mathrm{d}x = 0.04836$ rad/pixel. The statistical error for this least-squares fit is $\pm 0.00018$ rad/pixel. Since the phase in the specimen is measured with respect to the reference wave in vacuum, the flatness of the vacuum level ($\pm 0.00025$ rad/pixel) must also be added to the uncertainty of the measured slope resulting in a combined relative error of 0.9%. The combination of all these measurements gives a value of $V_0 = 14.13 \pm 0.17$ V for the bulk mean

inner potential of GaAs in the kinematical approximation. The statistical accuracy of 1.2% is dominated by specimen imperfections, by limited statistical accuracy of the phase measurement, and by uncertainty in the hologram magnification calibration.

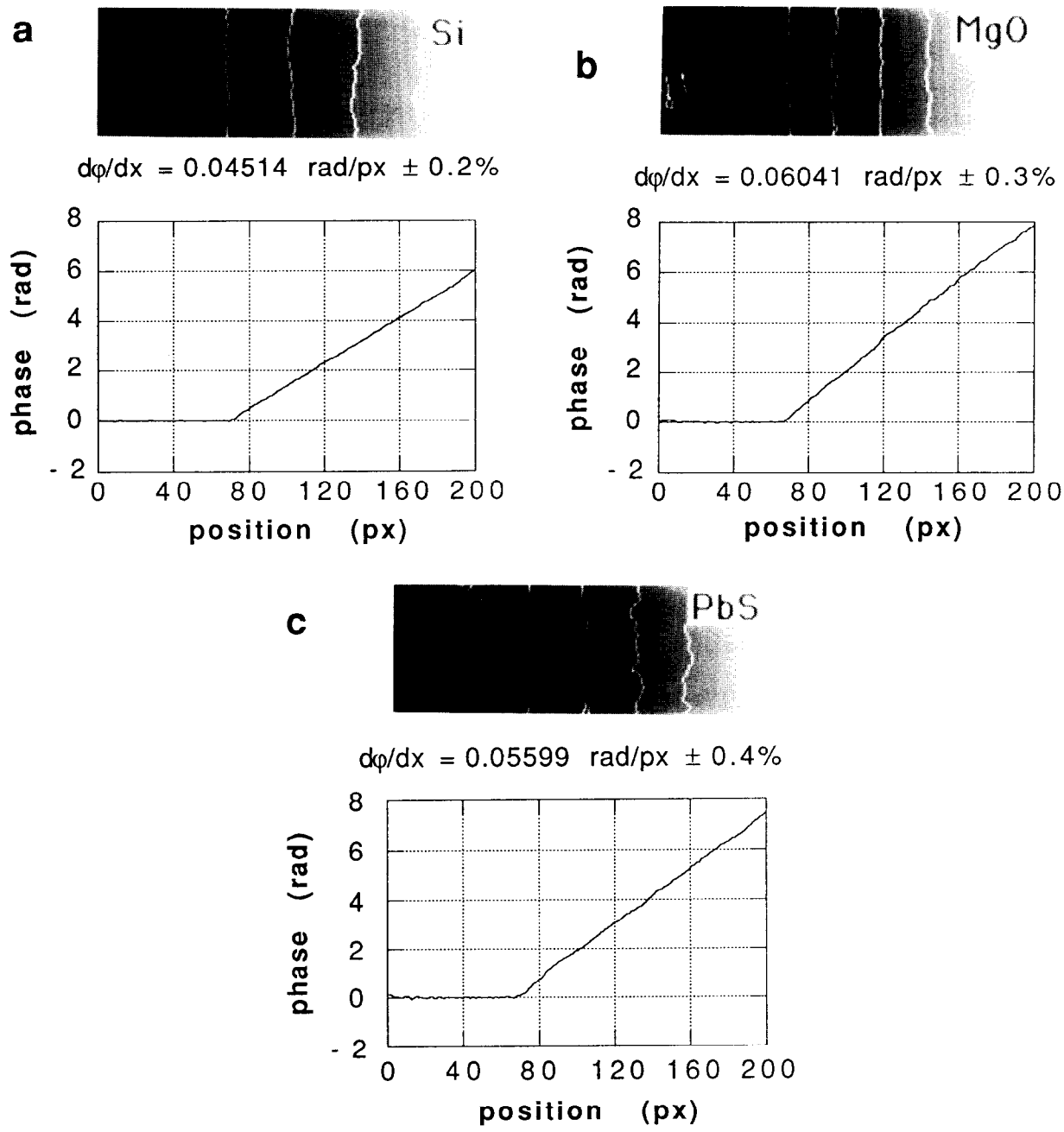


Fig. 6. Phase region and profile for: (a) Si wedge ($\theta = 109.5°$; $\alpha = 5.99°$; $\beta = 2.24°$); (b) MgO wedge ($\theta = 90°$; $\alpha = 22.12°$; $\beta = 2.60°$); and (c) PbS wedge ($\theta = 90°$; $\alpha = 4.07°$; $\beta = 3.21°$).

The same method was applied to wedges of Si, MgO and PbS. Examples of contoured phase regions, with equiphase lines at $\pi/2$ intervals, and phase profiles from representative holograms, are given in fig. 6. The measured phase slopes at the particular angles of crystal tilt are denoted in the figure (the magnification and electron energy being identical for all cases). The improved statistical accuracy of the phase slope measurements in the cases of Si, MgO and PbS is due to the larger vacuum region in the studied holograms, and less surface pitting compared to the GaAs sample used for the examples in figs. 2–5. The kinematical approximation yields for $V_0$: Si (9.11 V $\pm$ 0.5%); MgO (12.78 V $\pm$ 0.6%); PbS (16.35 V $\pm$ 0.7%). Because of the high statistical accuracy of these values, it is important to investigate the magnitude of systematic errors introduced by residual dynamical diffraction effects.

## 5. Dynamical diffraction effects

Are there kinematical orientations for crystals [24]? This question has been very important in analytical microscopy where diffraction effects are minimized by selecting "non-channeling orientations" as we have just attempted to do in the holograms from tilted crystals presented in section 4. Avoiding a low-index zone axis is an obvious choice, and the phase profiles from GaAs at [100] zone and Si at [100] and [111] zones, shown in fig. 7, illustrate this point. The phase change of the transmitted beam in the zone-axis case is introduced both by the mean inner potential and by dynamical scattering from the diffracted beams. The large phase jumps in fig. 7 coincide with the extinction contours in the amplitude images, as demonstrated by Hanszen [25]. There is a wealth of information about the non-zero terms of the Fourier transform of the potential in these experimental phase images, but for the purpose of measuring $V_0$ these orientations are to be avoided. In some fortuitous cases, like the GaAs 90° wedge at [100] zone (fig. 7a), the slope in the increasing parts of the phase profile yields the same value for $V_0$ as the tilted crystal case of fig. 5. Even in such circumstances, the tilted crystal case is a better choice for measurement of $V_0$ because of the larger number of data points in the phase profile where one could fit a line to measure the slope. It is interesting to note that the phase change due to double diffraction has an opposite sign compared to the phase change due to mean inner potential in all cases in fig. 7.

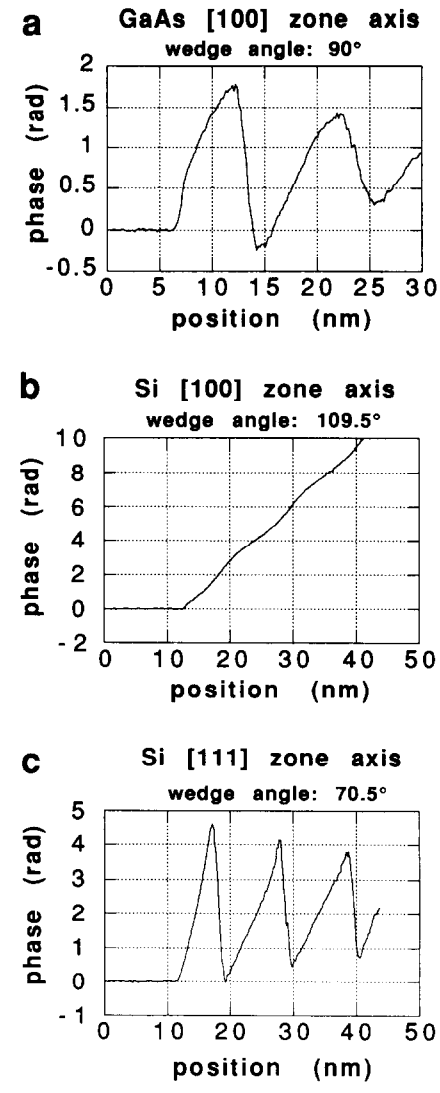


Fig. 7. Phase profiles from GaAs and Si wedges tilted to denoted zone axes show strong dynamical diffraction effects which modify the phase change due to mean inner potential.

To test the tilted crystal case, we have studied holograms from two different Si wedges obtained by cleavage from (111) and (100) wafers. In both cases, the crystals cleaved along (111) crystal planes resulting in 70.5° wedge mounted close to [111] zone and in 109.5° wedge close to [100] zone, respectively. The exact crystal orientations used in the holography experiments are given by the simulated kinematical CBED patterns in fig. 8. The corresponding experimental phase profiles are given in fig. 9 and the slopes obtained, converted to phase versus thickness for easier comparison, are denoted on each graph. The $(V_0)_{\text{kinematical}}$ values calculated with the kinemati-

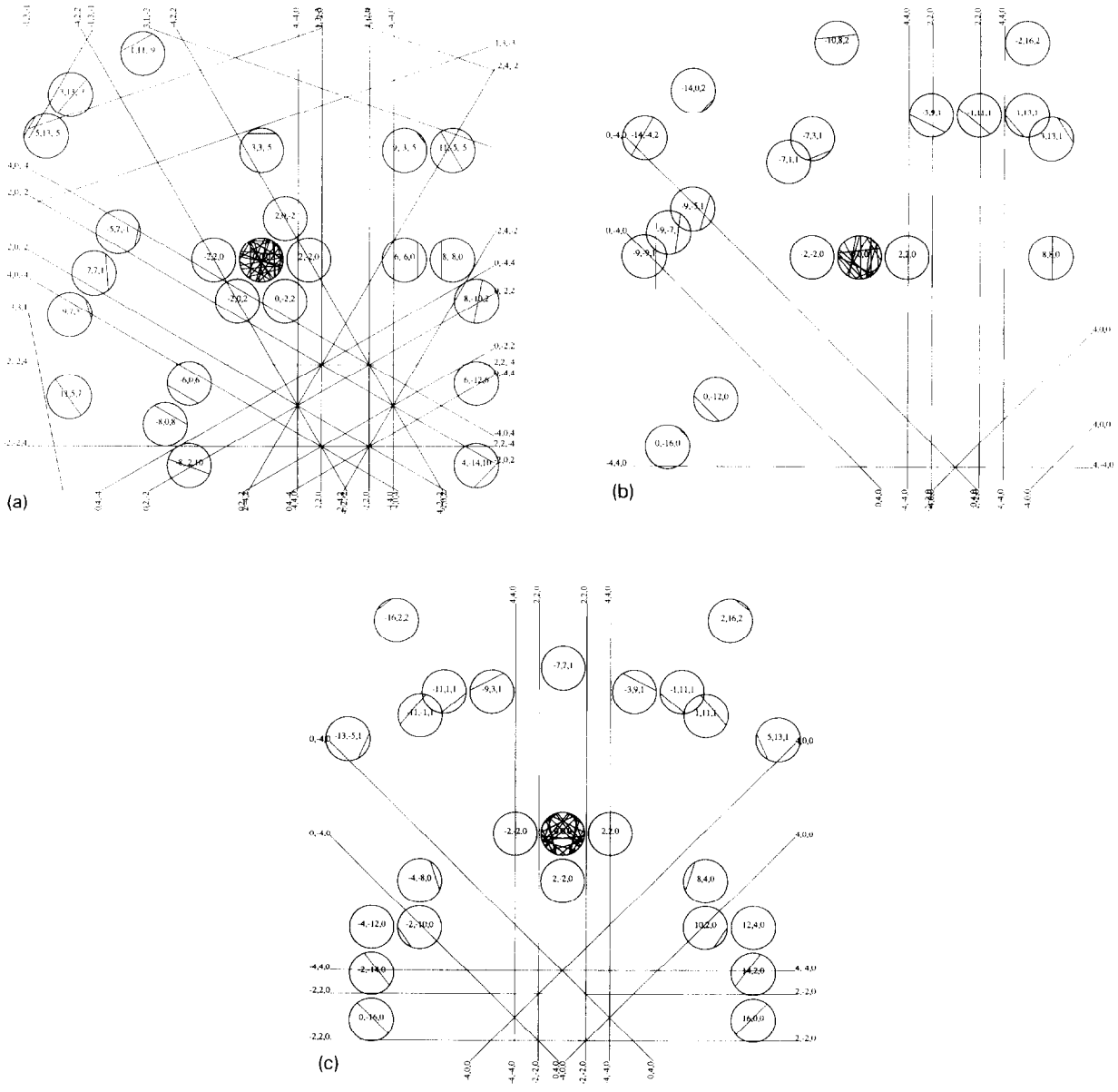


Fig. 8. (a–c) Simulated CBED patterns for three different orientations of Si wedges used for experimental holograms.

Table 1
Mean inner potential for Si crystal

| Si (fig. 8) | $(d\phi/dt)_{experimental}$ [rad/nm] (fig. 9) | $(V_0)_{kinematical}$ [V] | $(d\phi/dt)_{dynamical}$ [rad/nm] (fig. 10) | $V_0$ [V] |
|---|---|---|---|---|
| a | $0.08208 \pm 0.00043$ | $8.88 \pm 0.9\%$ | $0.003543 \pm 0.000007$ | $9.26 \pm 0.9\%$ |
| b | $0.08422 \pm 0.00014$ | $9.11 \pm 0.5\%$ | $0.001350 \pm 0.000003$ | $9.26 \pm 0.5\%$ |
| c | $0.09573 \pm 0.00040$ | $10.35 \pm 0.8\%$ | $-0.009558 \pm 0.000052$ | $9.32 \pm 0.9\%$ |

Phase change of transmitted electrons with thickness $(d\phi/dt)_{experimental}$, as measured from electron holograms of Si wedges in three orientations, is corrected for diffraction contribution by adding $(d\phi/dt)_{dynamical}$ from theoretical Bloch wave calculations. Resulting phase slope gives true mean inner potential $V_0$. Values without dynamical corrections $(V_0)_{kinematical}$ are included for comparison.

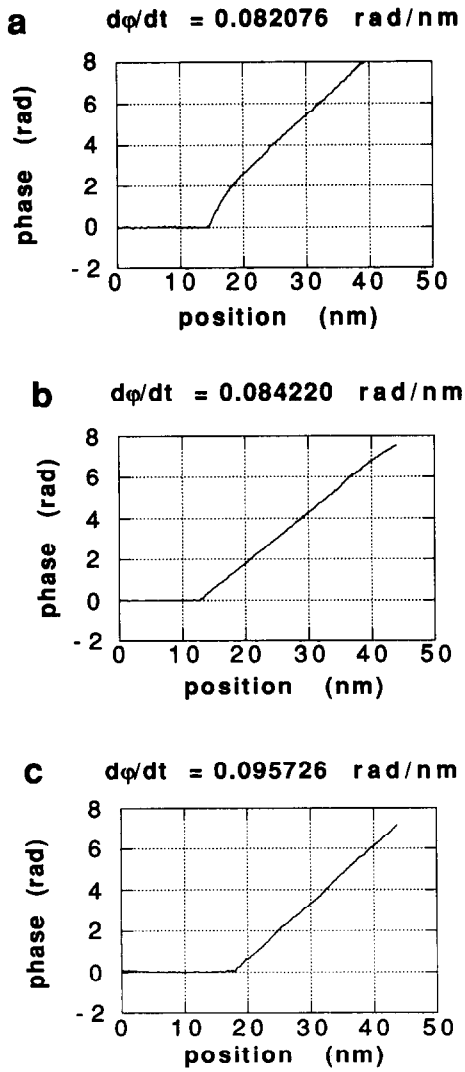


Fig. 9. Experimental phase profiles for Si wedges tilted as in fig. 8. Phase changes as function of thickness are denoted.

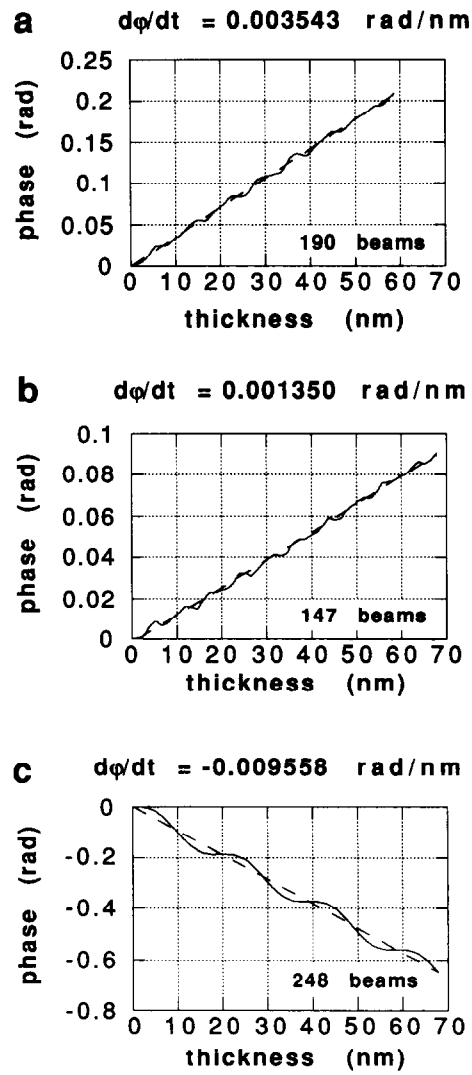


Fig. 10. Bloch wave calculations of dynamical contributions to phase of transmitted beam as function of Si crystal thickness for the tilts of fig. 8.

cal approximation from these slopes (eqs. (2)–(4)) are given in table 1. The results obtained for the first two cases (figs. 9a and 9b) vary by 2.6%. This suggests very small residual dynamical diffraction effects for these tilts where the major K bands are avoided. In the third case, when the transmitted beam is parallel to the {110} crystal planes, the slope changes by about 15%, demonstrating that planar channeling results in larger apparent inner potential. This case would be unavoidable for edge-on holographic studies of interfaces of epitaxial layers, because avoiding a zone axis can be done only to the extent of tilting parallel to the plane of the interface.

We have used Bloch wave calculations to correct for dynamical diffraction effects at the three orientations of Si shown in fig. 8. The computation program has been published [26] and includes absorption in the calculations. The absorption potential was computed with the ATOMS program [27] which uses the Einstein model for thermal vibrations, the Debye–Waller factor being the input parameter. For Si we used the DW factor at room temperature of 0.46. The number of beams in the calculations was increased until convergence of the results was reached, more beams being necessary for the planar channeling orientation of fig. 8c compared to the other two arbitrary tilts.

The phase of the transmitted beam was calculated as a function of thickness, as shown in fig. 10. The theoretical phase profiles in fig. 10 contain information only about the phase change of the transmitted beam due to dynamical contributions from the scattered beams, the mean inner potential being excluded from the calculations. It is therefore interesting to approximate the calculated phase profiles with a line and test whether the experimental phase profiles can be corrected for the dynamical diffraction contributions. The slopes calculated by linear fitting to the theoretical phase profiles are denoted on the graphs in fig. 10; their errors stated in table 1 were calculated from the statistical departure of the phase profiles from the fitted line. As in the zone-axis cases in fig. 7, the phase change due to dynamical diffraction is in opposite direction to the phase change due to the mean inner potential. Therefore, the experimental slopes obtained from holography can be corrected for diffraction effects by adding the theoretical slopes from the Bloch wave calculations. For Si in the three orientations studied, this correction results in very similar values for $V_0$ (table 1), the uncertainty remaining below 1% due to the small absolute values of the dynamical phase changes. It seems reasonable to conclude from this study that the dynamical diffraction contributions to the phase of the transmitted beam can be calculated and removed to yield the phase change caused only by the inner potential.

Bloch wave calculations were also performed for MgO, GaAs and PbS to estimate the validity of the kinematical approximation for the tilts used in the experimental phase images and profiles in figs. 5 and 6. Absorption was included in the calculations for MgO (0.346 and 0.315 were the respective room temperature DW factors for Mg and O [28]) and for GaAs (0.252 for DW of Ga and 0.266 for DW of As at 100 K [29]), but not in the calculations for PbS (we could not find a suitable DW value). The calculated phase profiles are given in fig. 11 along with the fitted slopes. These values were then used to correct for dynamical diffraction effects and to get the true values of the bulk inner potential for the materials studied, as summarized in table 2. The data in this table show that the kinematical approximation yields values for $V_0$ which are lower than the true values by less than 5% for the chosen crystal tilts.

## 6. Discussion

Comparison of our experimental results for $V_0$ with prior measurements confirms the general trend that the variations in the values obtained by different methods are often larger than the experimental errors of the individual measurements:

(i) Our value for Si of $9.26 \pm 0.08$ V differs substantially from $11.5 \pm 1$ V as obtained by measurements of refraction of Kikuchi lines in RHEED patterns from (111) surfaces of Si [13]. These RHEED experiments were performed on contaminated surfaces, however similar higher

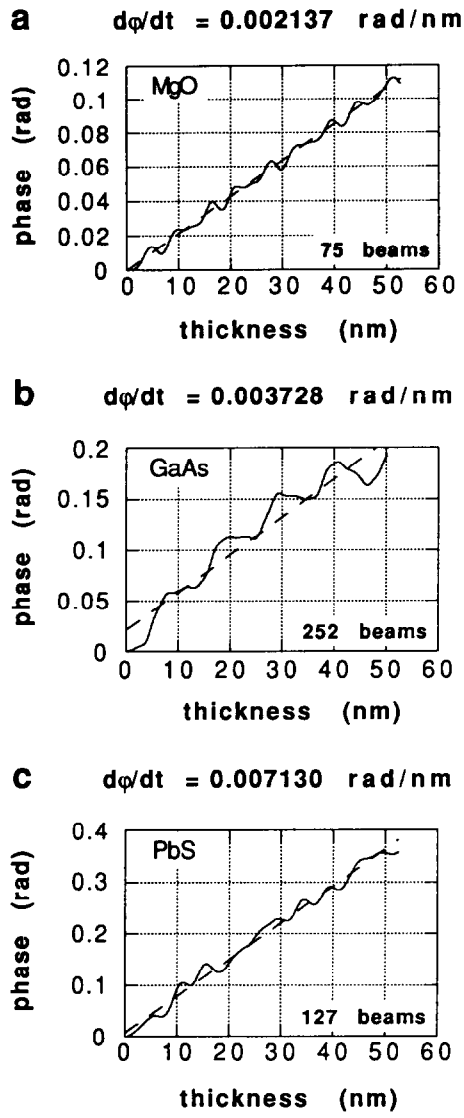


Fig. 11. Dynamical Bloch wave calculations of phase of transmitted beam as function of thickness of: (a) MgO; (b) GaAs and (c) PbS for tilts used in experimental holograms.

values for $V_0$ have been obtained in UHV RHEED rocking curve experiments from clean reconstructed (100) and (111) Si surfaces [30].

(ii) A larger number of measurements of $V_0$ have been performed from refraction effects in electron diffraction patterns of MgO with results ranging from 12.3 to 16 V (see table 1 in ref. [7] and references therein). Our holography result from cleaved MgO wedges of $V_0(\mathrm{MgO}) = 13.01 \pm 0.08$ V is at the lower end of this range, but coincides with the previous electron interferometry measurement from cleaved MgO ($13.2 \pm 1$ V) [18], and is close to the interferometric results from MgO smoke of $14.0 \pm 0.5$ V [16] and $13.5 \pm 0.85$ V [17]. Our value also agrees with theoretical calculations where the ionicity of Mg and O is taken into account [31].

(iii) Our result for GaAs of $14.53 \pm 0.17$ V is higher than the value of $13.2 \pm 0.6$ V obtained from RHEED patterns of cleaved (110) surfaces with steps [14]. The latter method measures the angular difference between the specular reflection from flat areas on the surface (electrons refracted both when entering and leaving the surface) and the corresponding Bragg reflection transmitted through a step (refracted only when entering the surface) and is therefore sensitive to surface contamination. Depending on the refractive index of the contamination layer, the result obtained for $V_0$ could be either lower or higher than the true value for the studied crystal.

Further studies are needed to establish whether there is a fundamental reason for the discrepancy between the RHEED and holography results, or if some specimen and experimental details are sources of the differences. The surface contributions to the bulk inner potential could fall in the first category, while surface con-

Table 2
Mean inner potentials $V_0$ for four crystals studied

| Crystal | $(\mathrm{d}\phi/\mathrm{d}t)_{\mathrm{experimental}}$ [rad/nm] (figs. 5 and 6) | $(V_0)_{\mathrm{kinematical}}$ [V] | $(\mathrm{d}\phi/\mathrm{d}t)_{\mathrm{dynamical}}$ [rad/nm] (fig. 10) | $V_0$ [V] |
|---|---|---|---|---|
| Si | See table 1 | | | $9.26 \pm 0.9\%$ |
| MgO | $0.11816 \pm 0.00035$ | $12.78 \pm 0.6\%$ | $0.002137 \pm 0.000007$ | $13.01 \pm 0.6\%$ |
| GaAs | $0.13064 \pm 0.00118$ | $14.13 \pm 1.2\%$ | $0.003728 \pm 0.000055$ | $14.53 \pm 1.2\%$ |
| PbS | $0.15118 \pm 0.00060$ | $16.35 \pm 0.7\%$ | $0.007130 \pm 0.000033$ | $17.19 \pm 0.7\%$ |

Mean inner potentials obtained by adding calculated phase change with thickness due to diffraction $(\mathrm{d}\phi/\mathrm{d}t)_{\mathrm{dynamical}}$ to phase slope $(\mathrm{d}\phi/\mathrm{d}t)_{\mathrm{experimental}}$ measured from electron holograms. Kinematical approximation applied to same experimental data results in lower $(V_0)_{\mathrm{kinematical}}$ values.

tamination, diffraction effects, specimen temperature, crystal impurities, etc., would need to be considered for the second. Holography from crystal wedges is not susceptible to surface contamination, and we have shown that the diffraction effects can be reduced and accounted for. Preliminary experiments with PbS wedges at room temperature and at liquid-nitrogen temperatures do not show differences which are larger than the experimental uncertainty of 0.7%. Further experiments are planned to determine whether crystal doping results in measurable changes of $V_0$.

## 7. Conclusions

We have developed a new method for measurement of mean inner potential of crystals by using cleaved crystal wedges and by applying digital image recording to electron holography. The inner potential of such crystal wedges can be quantified to statistical accuracies of about 1% which is a factor of three better than previous measurements. Dynamical diffraction effects are minimized by tilting away from strong diffracting conditions. The residual phase changes due to diffraction can be calculated with high accuracy and can be removed from the experimental phase profiles to obtain the value of the mean inner potential. Unlike the LEED and RHEED methods in which the surface states can contribute to the measured inner potential, this method determines the bulk mean inner potential. When combined with recent theoretical developments, this experimental method should provide a sensitive measure for the charge redistribution in crystals. By taking advantage of the high spatial resolution of electron microscopes, quantitative digital electron holography offers an exciting opportunity to study directly electrostatic potentials in nano-scale electronic structures.

## Acknowledgments

This work was performed in the Center for High-Resolution Electron Microscopy at Arizona State University supported by NSF grants DMR89-13384 and DMR91-15680 (J.M. Zuo was supported by NSF DMR90-15867). We are grateful to J.M. Cowley, A. Ichimiya, H. Lichte, M.A. O'Keefe, P. Rez, J.C.H. Spence and E. Völkl for stimulating discussions. R. Graham provided the GaAs sample and P. Perkes helped with computer setup for hologram reconstruction.

## References

[1] A. Tonomura, Rev. Mod. Phys. 59 (1987) 639.
[2] A. Tonomura, T. Matsuda, J. Endo, T. Arii and K. Mihama, Phys. Rev. Lett. 44 (1980) 1430.
[3] H. Lichte, in: Advances in Optical and Electron Microscopy, Vol. 12, Eds. T. Mulvey and C.J.R. Sheppard (Academic Press, London, 1991) p. 25
[4] R. Buhl, Z. Phys. 155 (1959) 395;
M. Keller, Z. Phys. 164 (1961) 274;
C. Jönsson, H. Hoffmann and G. Möllenstedt, Phys. Kondens. Mater. 3 (1965) 193;
H. Hoffmann and C. Jönsson, Z. Phys. 182 (1965) 360.
[5] W.J. de Ruijter and J.K. Weiss, Ultramicroscopy 50 (1993) 269.
[6] M. Gajdardziska-Josifovska, M.R. McCartney and J.K. Weiss, in: Proc. 50th Annual EMSA Meeting, Eds. G.W. Bailey, J. Bentley and J.A. Small (San Francisco Press, San Francisco, CA, 1992) p. 134.
[7] J.C.H. Spence, Acta Cryst. A 49 (1993) 231.
[8] S. Miyake, Proc. Phys.-Math. Soc. Jpn. 22 (1940) 666;
J.A. Ibers, Acta Cryst. 11 (1958) 178.
[9] P. Becker and P. Coppens, Acta Cryst. A 46 (1990) 254.
[10] M.A. Van Hove, W.H. Weinberg and C.-M. Chan, Low-Energy Electron Diffraction (Springer, Berlin, 1986) p. 132.
[11] J.B. Pendry, Low Energy Electron Diffraction (Academic Press, Boston, 1974) pp. 32, 262.
[12] L. Reimer, Transmission Electron Microscopy (Springer, Berlin, 1989) p. 57.
[13] K.H. Gaukler and R. Schwarzer, Optik 2 (1971) 215.
[14] N. Yamamoto and J.C.H. Spence, Thin Solid Films 104 (1983) 43.
[15] S. Miyake, K. Fujiwara and K. Suzuki, J. Phys. Soc. Jpn. 18 (1963) 1306.
[16] K. Yada, K. Shibata and T. Hibi, J. Electron Microsc. 22 (1973) 223.
[17] R.A. Herring, T. Tanji and A. Tonomura, in: Proc. 50th Annual EMSA Meeting, Eds. G.W. Bailey, J. Bentley and J.A. Small (San Francisco Press, San Francisco, CA, 1992) p. 990
[18] F. Sonier, J. Microscopie 12 (1971) 17.
[19] J.K. Weiss, W.J. de Ruijter, M. Gajdardziska-Josifovska, M.R. McCartney and D.J. Smith, Ultramicroscopy 50 (1993) 301.

[20] H. Lichte, Ultramicroscopy 20 (1986) 293;
E. Völkl and H. Lichte, Ultramicroscopy 32 (1990) 177.
[21] W.J. de Ruijter and J.K. Weiss, Rev. Sci. Instr. 63 (1992) 4314.
[22] W.J. de Ruijter, M. Gajdardziska-Josifovska, M.R. McCartney, R. Sharma, D.J. Smith and J.K. Weiss, in: Proc. 10th Pfeffercorn Conf., 1992, in press.
[23] J.M. Zuo, Ultramicroscopy 41(1992) 211.
[24] J.A. Eades, K.K. Christenson and M.L. Andreessen, in: Proc. 12th ICEM, Vol. 4, Eds. L.D. Peachey and D.W. Williams (San Francisco Press, San Francisco, CA, 1990) p. 412.
[25] K.-J. Hanszen, J. Phys. D (Appl. Phys.) 19 (1986) 373.
[26] J.C.H. Spence and J.M. Zuo, Electron Microdiffraction (Plenum, New York, 1992).
[27] D. Bird and Q.A. King, Acta Cryst. A 46 (1990) 202.
[28] T.M. Sabine, R.B. Von Dreele and J.E. Jørgsen, Acta Cryst. A 44 (1988) 374.
[29] J.S. Reid, Acta Cryst. A 39 (1983) 1.
[30] A. Ichimiya, private communication.
[31] M. O'Keefe and J.C.H. Spence, Acta Cryst. A, in press.